Open-Source CFD Simulation of Magnetic Rotating Swimmers with Experimental Validation

Yitong Lu¹, Jocelyn Ramos², Deeksha Sarda³, Dipan J. Shah⁴, Aaron T. Becker¹, and Julien Leclerc^{1*}

Abstract—Many potential medical applications for magnetically controlled tetherless devices inside the human body have been proposed, including procedures such as biopsies, blood clot removal, and targeted drug delivery. These devices are capable of wirelessly navigating through fluid-filled cavities in the body, such as the vascular system, eyes, urinary tract, and ventricular system, to reach areas difficult to access via conventional methods. Once at their target location, these devices could perform various medical interventions. This paper focuses on a special type of magnetic tetherless device called a magnetic rotating swimmer, which has internal magnets and propeller fins with a helical shape. To facilitate the design process, an automated geometry generation program using OpenSCAD was developed to create the swimmer design, while computational fluid dynamics simulations using OpenFOAM were employed to calculate the propulsive force produced by the swimmer. Furthermore, an experimental approach is proposed and demonstrated to validate the model. The results show good agreement between simulations and experiments, indicating that the model could be used to develop an automatic geometry optimization pipeline for rotating swimmers.

I. Introduction

Robotic magnetic manipulation is currently studied by several research groups for use in cardiac surgery. This technology could improve the control of catheters [1]-[4]. In this innovative method, the tip of a catheter contains a magnetic material. Large magnets placed around the patient produce a controlled magnetic field that generates a force or a torque on the magnetic material and helps guide the catheter [5], [6]. A tetherless variation of this method is also possible using Magnetic Tetherless Agents (MTAs). They are not yet used in the clinical realm but could be the next evolution of magnetically guided procedures. They have the potential to reduce the invasiveness of current procedures and enable new treatment paradigms. MTAs are objects that normally do not contain electronic sensors or complex mechanical parts, which make them easy to miniaturize. They are controlled via an external robotic system that generates a magnetic field to apply a torque or a force on the MTA itself [7]. The potential applications of these devices are numerous. They could operate in many areas of the body, such as the vascular system, the eye, the urinary tract, or the ventricular system, to deliver medication or perform surgical tasks.

This work was supported by the National Science Foundation under Grant Nos. [CPS-1932572, IIS-2130793].

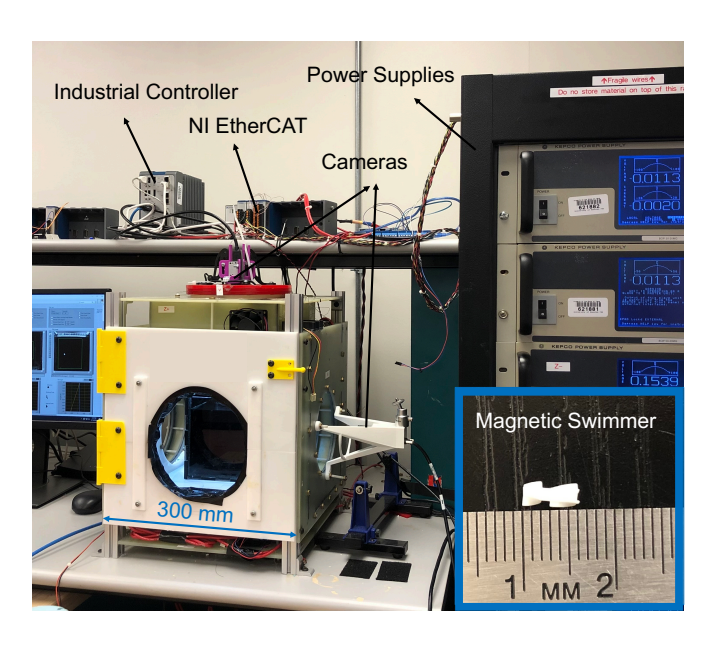


Fig. 1. Picture of the robotic magnetic manipulator used in this study. Inset: a rotating swimmer with a diameter of 3.2 mm and a length of 6 mm.

Miniature MTAs known as Rotating Swimmers (RSs) have been studied to abrade blood clots in vitro [8], [9]. RS contain magnetic material with radial magnetization. They are actuated wirelessly by a robotic magnetic manipulator that produces a rotating magnetic field. The RS's magnetic material interacts with the applied field, producing a torque that rotates the agent. RS has propeller fins or a spiral-shaped body that converts the rotational movement into a propulsive force [10]–[16]. Controlling the orientation of the magnetic field in the rotational plane enables 3D manipulation of these agents [17]–[23]. Figure 1 shows the robotic magnetic manipulator and one of the swimmer designs used in this paper.

The navigational abilities of an RS are dictated partly by its geometry, which influences drag, weight, buoyancy, and center of mass. These affect rotating swimmers' velocity, turning radius, size, and stability. The swimmer's performance requirements in terms of velocity and size could be defined by the location in the body where the procedure is performed. For example, RSs designed to navigate large arteries must produce enough propulsive force to counteract the pulsating flow, which can reach 100 mm s⁻¹ in the aorta. However, RSs designed to navigate through small vessels will be subjected to relatively low flow rates and may have tighter restrictions on size and magnet volume. The optimum geometry of an RS is also affected by the Reynolds number,

¹Electrical & Computer Engineering, University of Houston, TX, USA

²Mechanical Engineering, University of Houston, TX, USA

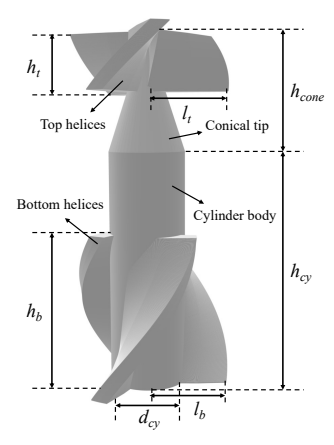
³School of Engineering Medicine, Texas A&M University, Houston, USA

⁴Houston Methodist DeBakey Heart & Vascular Center, TX, USA

^{*} Corresponding author. Email: jleclerc@central.uh.edu

 $TABLE\,\,I$ Parameters used in OpenSCAD to generate the swimmer designs used in Sections III and IV

Parameter name	Design A	Design B	Design C
CAD drawing			
Diameter of the cylinder body, d_{cy} [mm]	1.2	1.2	1.2
Height of the cylinder body, h_{cy} [mm]	4.0	4.0	4.0
Height of the conical tip, h_{cone} [mm]	2.0	2.0	2.0
Number of top helices, n_t	3.0	2.0	3.0
Number of bottom helices, n_b	3.0	4.0	3.0
Thickness of the top helices, l_t [mm]	1.0	1.0	1.0
Thickness of the bottom helices, l_b [mm]	1.0	1.0	1.0
Pitches of the top helices, p_t [mm]	15.0	12.0	8.0
Pitches of the bottom helices, p_b [mm]	15.0	15.0	8.0
Height of the top helices, h_t [mm]	1.5	2.5	1.0
Height of the bottom helices, h_b [mm]	1.5	1.5	2.6



which is a function of the velocity, the density of the fluid, the viscosity of the fluid, and the characteristic length of the RS. The fluid viscosity an RS navigates within could vary by subject and the location in the body it is traveling in.

In recent years, many studies on the RS's efficiency have been studied experimentally and through simulations [24]-[26]. Other works with Computational Fluid Dynamics (CFD) have studied how to improve the RS's swimming performances by varying different geometric parameters of the helix [27]-[29]. These works mainly focus on two geometrical aspects for optimizing RS's swimming performance: helical shape and helix cross-section. In this paper, we focus on the entire swimmer design, including the cylinder body, cone-shaped head, and helical shape, to analyze their combined effect on swimming. Furthermore, it is known that an essential non-geometric parameter that influences the swimmer's performance is magnetization. Therefore, we also studied the swimmers' performance with different sizes of permanent magnets embedded inside the swimmer cylinder body by considering the weight of the swimmer.

The main contribution of this paper is the creation of a free, open-source model for computing the force and torque produced by RSs using a finite element method. The code is available at [30]. This paper also presents a new experimental procedure to validate this model. The most accurate model will be used in our future research to optimize geometries depending on the requirement of the procedure to perform (fluid viscosity, velocity needed, etc.). The automatic geometry generation method is shown in Section II. The computational methods including two fluid dynamics models to compute the force produced by the swimmer are presented in Section III. Section IV presents the results of the experimental validation of the CFD model. Finally, the conclusion is in Section V.

II. SWIMMER GEOMETRY GENERATION AND FABRICATION

A. Automatic Geometry Generation

To facilitate the design process of magnetic swimmers, we implemented a program that generates the 3D shape of RSs

from parameters and saved it as a .stl file. This program will also be used to perform the automatic optimization of RS geometries in the future. The geometry generation function was built using OpenSCAD and Python. Parameters used to generate the swimmer design are listed in Table I. The total length and diameter of the swimmer are held constant at 6 mm and 3.2 mm, respectively. The length of the swimmer L is defined as $L = h_{cy} + h_{cone}$, where the height of the cylinder body h_{cy} and the height of the conical tip h_{cone} can be adjusted. The diameter of the swimmer D is defined as $D = d_{cy} + 2 \cdot \max(l_t, l_b)$, where the diameter of the cylinder body d_{cy} is chosen based on the size of the permanent magnet. The thickness of the top helices l_t and the thickness of the bottom helices l_b can be adjusted.

The parameters can be varied are: 1) the numbers of top helices n_t and bottom helices n_b , 2) the pitches of the top helices p_t and bottom helices p_b , and 3) the heights of the top helices h_t and bottom helices h_b . The parameters defined are altered with a Python script. Alterations of the original design are saved to a new file, and exported to .stl meshes for CFD computation.

Table I shows three representative swimmer designs used in Section III and Section IV. These three designs have the same diameter (same diameter of the cylinder body and thickness of the helices) and height (same height of cylinder body and conical tip). Swimmer design A has both three helices at the top and bottom with the pitches of the helices of 15 mm and the height of the helices of 1.5 mm. Swimmer design B has two top helices and four bottom helices. The height of the top helices is 2.5 mm with pitches of 12 mm, while the height of the bottom helices is 1.5 mm with pitches of 15 mm. Swimmer design C has both three helices at the top and bottom with the pitches of the helices of 8 mm. The height of the top helices of this design is 1 mm, and the height of the bottom helices is 2.6 mm.

B. Swimmer Fabrication

Once the swimmer geometry is generated, the swimmer is printed using a Formlabs resin 3D printer with layer thick-

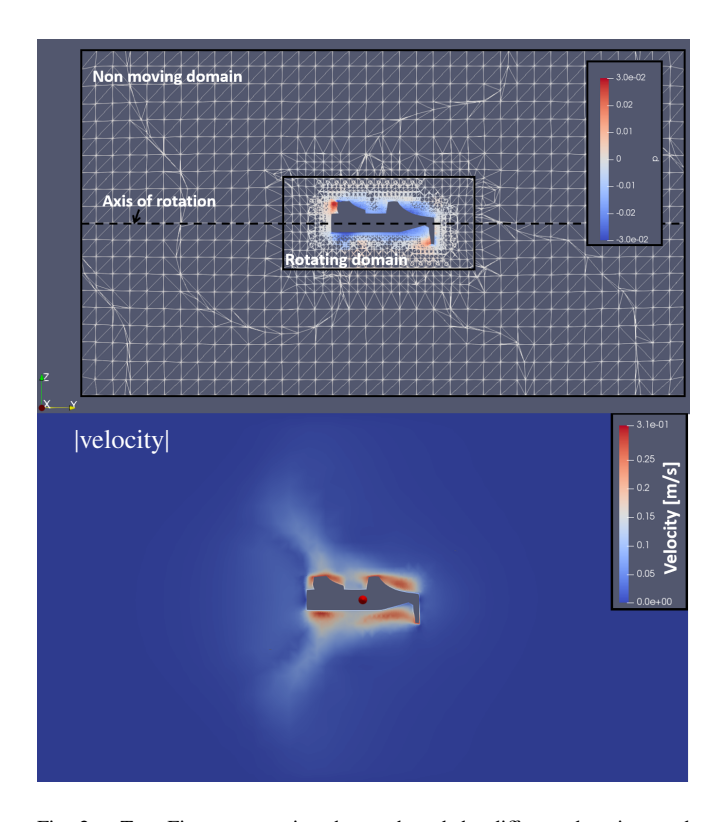


Fig. 2. Top: Figure presenting the mesh and the different domains used in the presented model. A typical pressure distribution calculated with the laminar model is also shown. Bottom: Distribution of the liquid velocity magnitude calculated using the laminar model.

ness of 0.05 mm. Then, the swimmer is cleaned using ethanol to remove the resin left on the surface of the swimmer and inside the hole that receives the magnet. After cleaning, the swimmer is placed under UV lights for 25 minutes to cure the resin. Two sizes of cylinder-shaped NdFeB permanent magnets are used in this study: one with a diameter of 1 mm and a length of 1.5 mm and another with a diameter of 0.75 mm and a length of 1 mm. The magnet is placed inside the hole at the bottom of the swimmer cylinder body. A small amount of epoxy is then added at the bottom to ensure that the magnet stays in place.

III. COMPUTATIONAL METHODS

A. OpenFOAM CFD Model

In this study, we simulated the RS in a cylindrical domain. The pimpleFoam solver of OpenFOAM was used. Two models were utilized to compute the propulsive force created by the swimmer: a laminar model and a k- ω -SST model. PimpleFoam is a transient solver for incompressible flows. The mesh was split into two domains: an internal cylindrical domain that rotates (this domain includes the swimmer's boundary) and an external cylinder mesh that does not move (see figure 2). Boundary conditions need to be defined in the front, back, and side of the non-moving cylinder as well as on the surface of the swimmer. The Dynamic Mesh feature of OpenFOAM was used to simulate the rotation of the swimmer. The computation was stopped

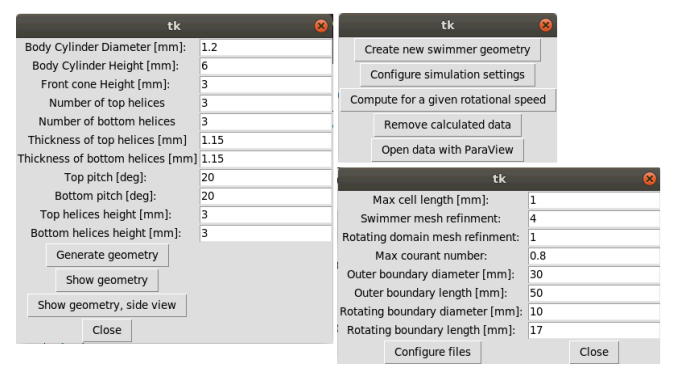


Fig. 3. Images showing the graphical user interface created.

when the force on the swimmer did not vary by more than 1% during one rotation of the swimmer. This indicates that the simulation reached a steady state. An image of a representative simulation result computed via OpenFOAM is shown in Fig. 2.

1) Laminar model: The laminar model of OpenFOAM only requires the definition of one physical constant regarding the fluid properties. It is the kinematic viscosity and, in our case, it was set to 9.34×10^{-7} Pa s, which corresponds to the dynamic viscosity of water at 23 °C. This temperature was chosen because this is the temperature at which experiments are performed in this paper.

The boundary conditions for the laminar model need to define the value of the fluid's velocity and pressure. The velocity of the fluid on the external boundary was set to $\vec{V} = V_s \cdot \vec{U}_y$ where V_s is the swimmer's forward velocity and \vec{U}_y is the unit vector along axis y. On the surface of the swimmer, the *movingWallVelocity* function of OpenFOAM was used. The pressure was set to 0 on the external wall that faces the back of the swimmer and to a fixed gradient with value 0 on all other boundaries.

2) k-omega-SST model: The k- ω -SST (Shear Stress Transport) model is a widely used turbulence model in computational fluid dynamics. It is a two-equation model that combines the best attributes of two popular models, the k- ω and the k- ε models.

The parameters that need to be defined in this model are the turbulent kinetic energy k, the turbulence dissipation rate ε , and the specific turbulence dissipation ω . Values of these parameters were obtained using an online calculator provided by Wolf Dynamics.

The boundary conditions for the pressure and velocity are the same as for the laminar model. The value of k was set to zero on all boundaries except on the surface of the swimmer where the OpenFOAM kqRWallFunction was used with a value of $6 \times 10^{-4} \, \text{m}^2/\text{s}^2$. The value of ε was set to $0.025 \, \text{m}^2/\text{s}^2$ everywhere. The value of ω was set to the constant value of $466 \, \text{m}^2/\text{s}^2$ everywhere except on the surface of the swimmer where the OpenFOAM function omegaWallFunction was used with a value of $466 \, \text{m}^2/\text{s}^2$.

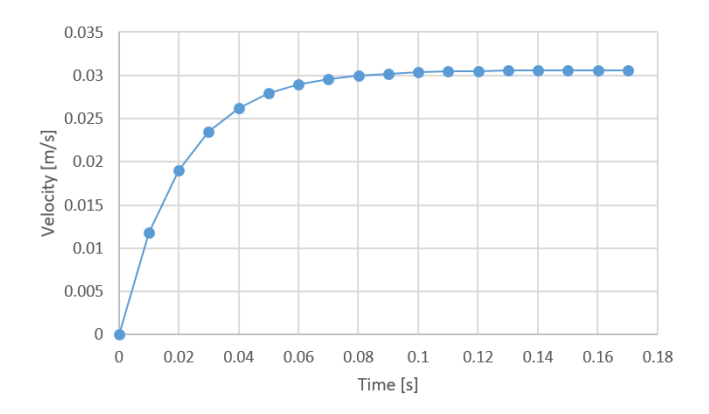


Fig. 4. Plot of a simulated swimmer velocity as a function of time. Design B with a mass of 15 mg was simulated moving vertically at a constant rotational speed of 45Hz.

B. Graphical Interface

A Linux Graphical User Interface (GUI) was created and is provided at [30]. The GUI allows setting many simulation settings, such as the size of the boundaries, the mesh refinement, the maximum courant number, and the maximum cell size. The GUI also allows starting a simulation to computer the force and torque produced by the swimmer at a user-defined rotational speed. Additionally, the GUI can launch the open-source display software ParaView included with OpenFOAM, and automatically load the results. Finally, the GUI allows the creation of swimmer geometries with user-defined properties (see Section II). Screenshots of the GUI are provided in Fig. 3.

The GUI was programmed using the language Python and the GUI toolkit Tkinter. Additional free Python packages such as NumPy and Matplotlib are also required. OpenFOAM 9 must be installed, and commands such as blockMesh, surfaceFeatures, and snappyHexMesh pimplefoam must be functional in terminals. OpenSCAD must be installed to generate swimmer geometries. Instructions to install the required software components are provided in the readMe file of the shared GitHub repository [30].

C. Vertical Movement Simulation

To demonstrate the capabilities of the model, we utilized it to compute the motion of a magnetic swimmer as a function of time (see Fig. 4). The swimmer starts with zero velocity and rotates at a constant speed. The relative motion of the fluid around the swimmer is applied by setting a non-zero velocity along the y-axis (the axis of rotation of the swimmer) on the external boundaries. Additionally, various parameters were set, such as mass, initial position, time step size, and total simulation time.

Newton's second law was solved numerically using Euler's method, where acceleration was computed by dividing the produced force by the mass of the swimmer. The velocity and position of the swimmer were then updated iteratively using Euler's method within a loop, and re-computing the acceleration at each time step.

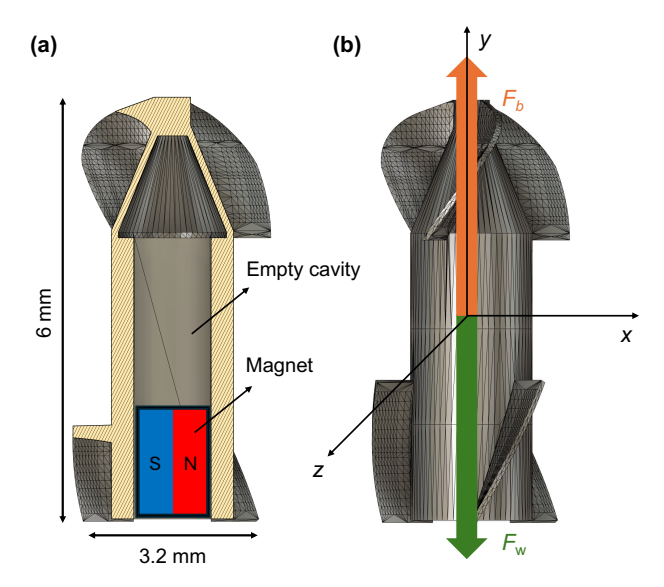


Fig. 5. (a) Cross-sectional view of the primary swimmer design with the internal magnet and the empty cavity. (b) The ideal force diagram of the swimmer is used to calculate vertical static force \vec{F}_{VSF} .

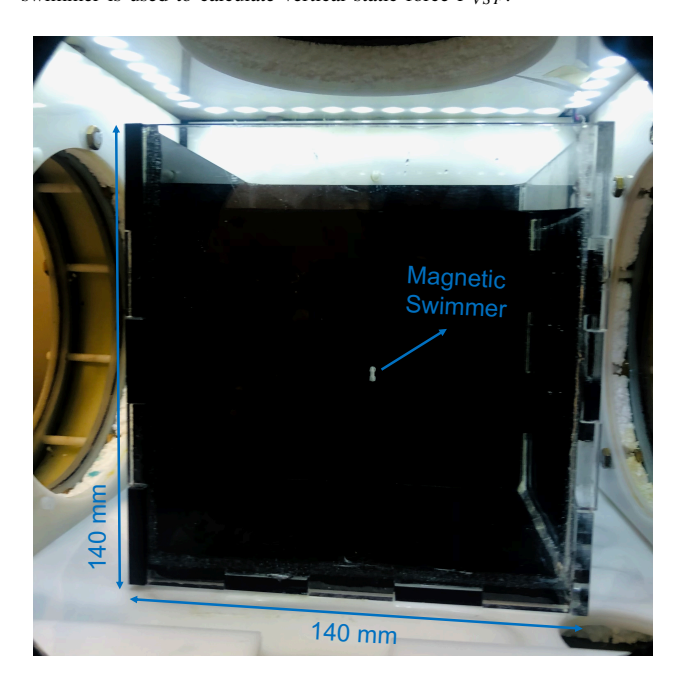


Fig. 6. The picture shows a magnetic rotating swimmer hovering in the center of a water tank placed inside the magnetic manipulator. The hovering frequency of this swimmer is 32 Hz.

IV. Experimental Validation of the model

A. Experimental Apparatus

Experimental measurements were performed using the magnetic manipulator described in [1] (see Fig. 1). The system has six electromagnets arranged in a cube shape. Each electromagnet is powered by a set of two Kepco 20-50 MG power supplies connected in series. The current in the electromagnets is controlled by a National Instrument IC3173 industrial controller. Two cameras on the top and right side of the manipulator monitor the workspace and allow the real-time measurement of the swimmer's position

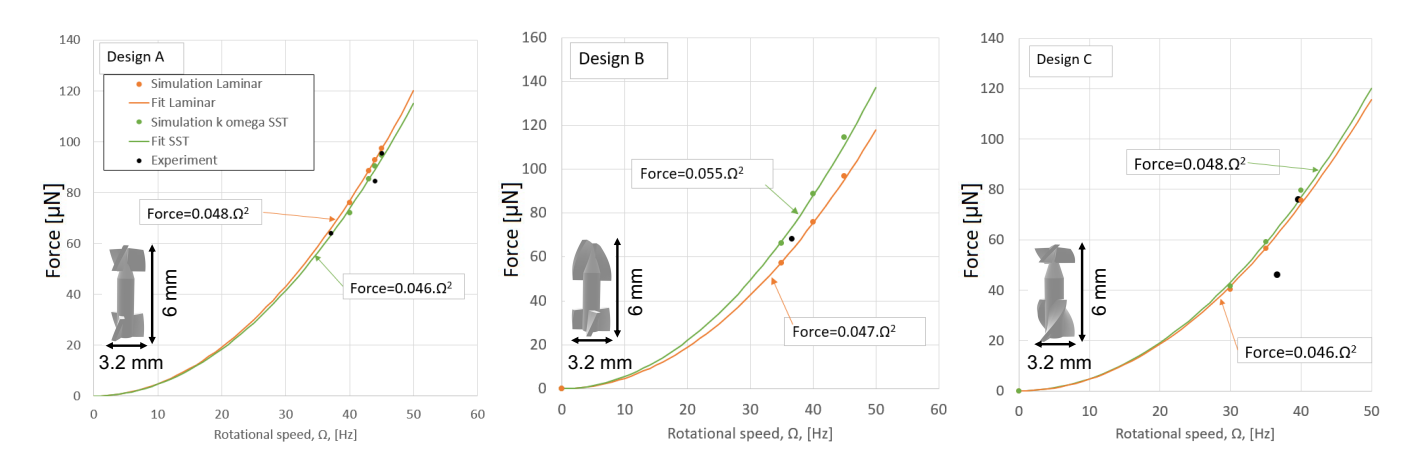


Fig. 7. Comparison between the force computed via OpenFOAM and experimental measurements for three different swimmer designs.

by detecting the brightest point on the image with a defined boundary size. The camera feedback is used to perform a closed-loop control of the swimmer. A 140 mm×140 mm water tank is placed in the center of the manipulator for testing the swimmer's swimming performance in a fluid environment.

B. Hovering Frequency Experimental Measurement

Measuring the force produced by a rotating magnetic swimmer is challenging because the swimmer's propulsive force is small (less than 1 mN), and the swimmer is tetherless. In this section, we present a method to measure the rotational frequency needed for a RS to produce a known amount of force.

RSs have a characteristic rotational speed that we call the *Hovering Frequency*. At this frequency, the swimmer can hover when oriented vertically, and the propulsive force exactly compensates the vertical static force \vec{F}_{VSF} , which is the vectorial sum of weight \vec{F}_W and buoyancy \vec{F}_b (see Fig. 5). The hovering frequency is measurable, and the force produced at this frequency can be calculated with the following equation:

$$\vec{F}_{VSF} = \vec{F}_b + \vec{F}_W \ . \tag{1}$$

Multiple points of the force-rotational speed characteristic of an RS can be obtained by measuring the hovering frequency of multiple RS having the same geometry but different masses. In this study, we varied the weight of our RSs by changing the volume of an empty cavity inside the agent and also the size of the internal permanent magnet (see Fig. 5). The weight and force of buoyancy are found with the respective masses m and volumes V:

$$\vec{F}_W = m \cdot \vec{g} ,$$

$$\vec{F}_b = \rho_{\text{liquid}} \cdot V \cdot \vec{g} , \qquad (2)$$

where \vec{g} is the acceleration of gravity and ρ_{liquid} is the liquid's density. We measured the mass of each RS using an analytical balance, and the volume was calculated using CAD software.

To measure the hovering frequency, each RS was placed in the water tank, and the magnetic field was applied with a rotational frequency starting from 15 Hz, then increased until the swimmer took off (see Fig. 6). Cameras were used to track the swimmer's position in the water tank, and a PID controller was utilized to control the rotation speed and keep the swimmer at a constant vertical position. The rotational speed was recorded for 250 data points and averaged to obtain an experimental measurement of hovering frequency. The corresponding propulsive force was then calculated using Eq. (1).

C. Validation Results

Figure 7 shows the comparison between the simulation and experimental results. The force computed from Open-FOAM simulation and the force calculated based on the experimental measurements were compared. Three different swimmer designs shown in Table I were used to validate the model. The experimental measurements are in good agreement with the force predicted using OpenFOAM. Trendlines were calculated to interpolate between the points calculated by simulation. The equations of the trendlines are shown in Fig. 7.

V. Conclusion

This paper presents and studies two different fluid dynamics models (laminar model and k- ω -SST model) to compute the force produced by a rotating swimmer. The paper also introduces an experimental method to validate the models. Simulation and experiment were validated using multiple swimmer geometries, and the validation results demonstrated good agreement between the simulation and experimental results. The open-source programs OpenSCAD and Open-FOAM were used, and the configured files, as well as a graphical interface, are available at [30].

Future work considers using these models to accelerate the development of magnetic rotating swimmers by offering a free solution to estimate the performance of swimmer designs. These models can also be used to create an automatic geometry optimization pipeline for the swimmers for different surgical applications.

REFERENCES

- [1] J. Leclerc, B. Isichei, and A. T. Becker, "A magnetic manipulator cooled with liquid nitrogen," *IEEE Robotics and Automation Letters*, vol. 3, no. 4, pp. 4367–4374, 2018.
- [2] A. W. Mahoney, J. C. Sarrazin, E. Bamberg, and J. J. Abbott, "Velocity Control with Gravity Compensation for Magnetic Helical Microswimmers," *Advanced Robotics*, vol. 25, no. 8, pp. 1007–1028, jan 2011. [Online]. Available: https://www.tandfonline.com/doi/full/ 10.1163/016918611X568620
- [3] B. Isichei, "Robotic Manipulators: Cryogenic Magnetic Manipulation System, Two-body Mag- netic Manipulation, and Low-cost Robotic Manipulators," Master's thesis, University of Houston, Dept. of Electrical & Computer Engineering, N308 Engineering Bldg 1, 4726 Calhoun Rd, 2018.
- [4] B. Conrad and M. Zinn, "Closed loop task space control of an interleaved continuum-rigid manipulator," in 2015 IEEE International Conference on Robotics and Automation (ICRA). IEEE, 2015, pp. 1743–1750.
- [5] J. Hwang, J.-y. Kim, and H. Choi, "A review of magnetic actuation systems and magnetically actuated guidewire-and catheter-based microrobots for vascular interventions," *Intelligent Service Robotics*, vol. 13, pp. 1–14, 2020.
- [6] M. E. Tiryaki, Y. G. Elmacıoğlu, and M. Sitti, "Magnetic guidewire steering at ultrahigh magnetic fields," *Science Advances*, vol. 9, no. 17, p. eadg6438, 2023.
- [7] C. Hong, Z. Ren, C. Wang, M. Li, Y. Wu, D. Tang, W. Hu, and M. Sitti, "Magnetically actuated gearbox for the wireless control of millimeter-scale robots," *Science robotics*, vol. 7, no. 69, p. eabo4401, 2022.
- [8] J. Leclerc, Y. Lu, A. T. Becker, M. Ghosn, and D. J. Shah, "Resonating magnetic manipulation for 3d path-following and blood clot removal using a rotating swimmer," in 2020 IEEE/RSJ International Conference on Intelligent Robots and Systems (IROS). IEEE, 2020, pp. 3083– 3090
- [9] I. S. Khalil, A. Adel, D. Mahdy, M. M. Micheal, M. Mansour, N. Hamdi, and S. Misra, "Magnetic localization and control of helical robots for clearing superficial blood clots," *APL bioengineering*, vol. 3, no. 2, p. 026104, 2019.
- [10] K. E. Peyer, S. Tottori, F. Qiu, L. Zhang, and B. J. Nelson, "Magnetic Helical Micromachines," *Chemistry - A European Journal*, vol. 19, no. 1, pp. 28–38, jan 2013. [Online]. Available: http://doi.wiley.com/10.1002/chem.201203364
- [11] J. J. Abbott, K. E. Peyer, M. C. Lagomarsino, L. Zhang, L. Dong, I. K. Kaliakatsos, and B. J. Nelson, "How Should Microrobots Swim?" *The International Journal of Robotics Research*, vol. 28, no. 11-12, pp. 1434–1447, nov 2009. [Online]. Available: http://journals.sagepub.com/doi/10.1177/0278364909341658
- [12] F. Ullrich, F. Qiu, J. Pokki, T. Huang, S. Pane, and B. J. Nelson, "Swimming characteristics of helical microrobots in fibrous environments," in 2016 6th IEEE International Conference on Biomedical Robotics and Biomechatronics (BioRob). IEEE, jun 2016, pp. 470–475. [Online]. Available: http://ieeexplore.ieee.org/document/7523671/
- [13] T. Xu, G. Hwang, N. Andreff, and S. Regnier, "Modeling and Swimming Property Characterizations of Scaled-Up Helical Microswimmers," *IEEE/ASME Transactions on Mechatronics*, vol. 19, no. 3, pp. 1069–1079, jun 2014. [Online]. Available: http://ieeexplore.ieee.org/document/6553581/
- [14] Huaming Li, Jindong Tan, and Mingjun Zhang, "Dynamics modeling and analysis of a swimming microrobot for controlled drug delivery," in *Proceedings 2006 IEEE International Conference on Robotics* and Automation, 2006. ICRA 2006. IEEE, 2006, pp. 1768–1773. [Online]. Available: http://ieeexplore.ieee.org/document/1641962/
- [15] F. Z. Temel and S. Yesilyurt, "Magnetically actuated micro swimming of bio-inspired robots in mini channels," in 2011 IEEE International Conference on Mechatronics. IEEE, apr 2011, pp. 342–347. [Online]. Available: http://ieeexplore.ieee.org/document/5971307/
- [16] W. Gao, X. Feng, A. Pei, C. R. Kane, R. Tam, C. Hennessy, and J. Wang, "Bioinspired Helical Microswimmers Based on Vascular Plants," *Nano Letters*, vol. 14, no. 1, pp. 305–310, jan 2014. [Online]. Available: http://pubs.acs.org/doi/10.1021/nl404044d
- [17] F. Z. Temel, A. E. Bezer, and S. Yesilyurt, "Navigation of mini swimmers in channel networks with magnetic fields," in 2013 IEEE International Conference on Robotics and Automation.

- IEEE, may 2013, pp. 5335–5340. [Online]. Available: http://ieeexplore.ieee.org/document/6631341/
- [18] T. Xu, G. Hwang, N. Andreff, and S. Regnier, "Characterization of three-dimensional steering for helical swimmers," in 2014 IEEE International Conference on Robotics and Automation (ICRA). IEEE, may 2014, pp. 4686–4691. [Online]. Available: http: //ieeexplore.ieee.org/document/6907544/
- [19] T. Xu, G. Hwang, N. Andreff, and S. Régnier, "Planar path following of 3-d steering scaled-up helical microswimmers," *IEEE Transactions* on *Robotics*, vol. 31, no. 1, pp. 117–127, Feb 2015.
- [20] A. Hosney, A. Klingner, S. Misra, and I. S. M. Khalil, "Propulsion and steering of helical magnetic microrobots using two synchronized rotating dipole fields in three-dimensional space," in 2015 IEEE/RSJ International Conference on Intelligent Robots and Systems (IROS). IEEE, sep 2015, pp. 1988–1993. [Online]. Available: http://ieeexplore.ieee.org/document/7353639/
- [21] K. Ishiyama, K. Arai, M. Sendoh, and A. Yamazaki, "Spiral-type micro-machine for medical applications," in MHS2000. Proceedings of 2000 International Symposium on Micromechatronics and Human Science (Cat. No.00TH8530). IEEE, 2000, pp. 65–69. [Online]. Available: http://ieeexplore.ieee.org/document/903292/
- [22] S. Lee, S. Lee, S. Kim, C.-H. Yoon, H.-J. Park, J.-y. Kim, and H. Choi, "Fabrication and characterization of a magnetic drilling actuator for navigation in a three-dimensional phantom vascular network," *Scientific reports*, vol. 8, no. 1, p. 3691, 2018.
- [23] X. Wu, J. Liu, C. Huang, M. Su, and T. Xu, "3-d path following of helical microswimmers with an adaptive orientation compensation model," *IEEE Transactions on Automation Science and Engineering*, 2019.
- [24] T. Xu, J. Yu, C.-I. Vong, B. Wang, X. Wu, and L. Zhang, "Dynamic morphology and swimming properties of rotating miniature swimmers with soft tails," *IEEE/ASME Transactions on Mechatronics*, vol. 24, no. 3, pp. 924–934, 2019.
- [25] T. Xu, G. Hwang, N. Andreff, and S. Régnier, "Modeling and swimming property characterizations of scaled-up helical microswimmers," IEEE/ASME Transactions on Mechatronics, vol. 19, no. 3, pp. 1069–1079, 2013.
- [26] J. Miao, X. Li, B. Liang, J. Wang, and X. Xu, "Enhancing swimming performance by optimizing structure of helical swimmers," *Sensors*, vol. 21, no. 2, p. 494, 2021.
- [27] J. E. Quispe, A. Bolopion, P. Renaud, and S. Régnier, "Enhancing swimming and pumping performance of helical swimmers at low reynolds numbers," *IEEE Robotics and Automation Letters*, vol. 6, no. 4, pp. 6860–6867, 2021.
- [28] J. E. Quispe, A. Oulmas, and S. Régnier, "Geometry optimization of helical swimming at low reynolds number," in 2019 International Conference on Manipulation, Automation and Robotics at Small Scales (MARSS). IEEE, 2019, pp. 1–6.
- [29] A. F. Tabak and S. Yesilyurt, "Computationally-validated surrogate models for optimal geometric design of bio-inspired swimming robots: Helical swimmers," Computers & Fluids, vol. 99, pp. 190–198, 2014.
- [30] Robotic Swarm Control Lab Github, "Magnetic Swimmer Simulator," 2024. [Online]. Available: https://github.com/RoboticSwarmControl/ swimmerCFDcode.